Electronic Supporting Information (ESI†)

Blooming nanoflowers on N, S-codoped microporous carbon nanobelts as oxygen reduction catalyst

Wenxiu Yang, Lulu Chen, Xiangjian Liu, Xiaoyu Yue, Changyu Liu, and Jianbo Jia *

State Key Laboratory of Electroanalytical Chemistry, Changchun Institute of Applied Chemistry, Chinese Academy of Sciences, Changchun 130022, China

University of Chinese Academy of Sciences, Beijing 100049, China

Corresponding Authors: jbjia@ciac.ac.cn (J. Jia)

Experimental Section

Materials: Carbon-supported Pt catalyst (20 wt %, Pt/C) was bought form Johnson Matthey. Polyvinylpyrrolidone (PVP) (M_W = 1300000), Pluronic® F127 (F127), and Nafion (5 wt %) were purchased from Sigma–Aldrich. Potassium chloride (KCl), zinc chloride ($ZnCl_2$), and ethanol were purchased from Beijing Chemical Reagent Company (Beijing, China). All chemicals were analytical grade and used as received. All aqueous solutions were prepared with ultrapure water from a Water Purifier System (Sichuan Water Purifier Co. Ltd., China).

Apparatus: X-Ray diffraction data were obtained with model D8 ADVANCE (BRUKER, Cu Kα radiation, λ =1.5406 Å). Scanning electron microscopy (SEM) images were obtained from an XL 30 ESEM FEG SEM (Philips, Netherlands). Transmission electron microscopy (TEM) was measured with a JEM-2100F high-resolution transmission electron microscope (JEOL Ltd., Japan). X-ray photoelectron spectroscopy (XPS) and ultraviolet photoelectron spectroscopy (UPS) studies of the resulting materials were performed using Thermo ESCALAB 250. For the XPS analysis, monochromatic AlKα (hγ = 1486.6 eV) excitation was employed. For the UPS analysis, a He lamp was used with 21.2 eV (He (I)) excitation energies. Nitrogen sorption isotherms were obtained with an ASAP 2020 Physisorption Analyzer (Micrometrics Instrument Corporation). Surface-enhanced Raman scattering (SERS) spectra were measured with a Renishaw 2000 model confocal microscopy Raman spectrometer with a CCD detector and a holographic notch filter (Renishaw Ltd., Gloucestershire, U.K.). The electrochemical experiments were employed using a CHI842B electrochemical workstation (CH Instruments, Shanghai). Rotating ring-disk electrode (RRDE) techniques were performed on a Model RRDE-3A Apparatus (ALS, Japan) with

CHI842B electrochemical workstation. The electrochemical experiments were performed through a three electrode system with a modified glassy carbon electrode (GCE) as the working electrode, an Ag/AgCl (saturated KCl) electrode as the reference electrode, and counter electrode (platinum foil), respectively. All the electrochemical measurements were carried out at room temperature.

Synthesis of the N, S-codoped carbon nanobelt composites: To prepare the electrospinning solution, ethanol was used as the solvent of PVP and F127. A mixture containing 20 ml PVP (0.10 g/ml) and 1.0 ml F127 (0.10 g/ml) was magnetically stirred at room temperature, and then 2.0 ml $ZnCl_2$/ KCl (n:n=1:1) aqueous solution was added into the above solution, and stirred overnight and used as the electrospinning precursor.

The electrospinning precursor was filled into a clean and dry plastic syringe with 7-gauge needle which was connected to a High Voltage DC Power Supply (Dongwen, Tianjin). A constant volume flow rate was controlled via a syringe pump (KDS 100, KD–Scientific). The aluminum foil was chose as a collector. The applied voltage was 13 kV, the flow rate was 1.0 mL/h, and the distance between the nozzle tip and the collector was 18 cm. Subsequently, heat treatments were produced with the electrospun nanobelts at 180 and 240 °C in a muffle at a heating rate of 2 °C min^{-1} for 2 h, respectively. Finally, the nanobelts were carbonized at 240 and 800 °C and held at that temperature for 3 and 1 h in N_2 with sublimed sulphur (S).

The above resulting sample was soaked in deionized water for 24 h and washed several times with deionized water to remove the salt template, and at last, dried it before use. For simplicity, the as-prepared samples were denoted as S-0.1-PFKZ, representing the addition of 0.1 gram of S, PVP, and F127, KCl and $ZnCl_2$.

For comparison, the PFKZ was also got without S element doping. The nanofiber from electrospinning of the PVP and F127 (PF) was also produced without KCl and $ZnCl_2$, while PFK was made from PVP, F127, and KCl (without $ZnCl_2$).

Electrocatalytic activity evaluation: Before modification, the GCE was polished carefully with 0.3 μm alumina slurries, followed by sonication in acetone, ethanol and ultrapure water successively, and then allowed to dry at room temperature. For a typical procedure, 6.0 mg of the S-0.1-PFKZ sample or Pt catalyst (20 wt %, Pt/C) were dissolved in a mixture (3 ml) of water, isopropyl alcohol, and Nafion (5.0 wt %) with a ratio of 20:1:0.075 (v/v/v) under sonication, respectively. For electrochemical measurements, a certain amount of the S-0.1-PFKZ suspension

was dropped onto the pretreated electrode surface (857 μg/cm^2), and the modified electrode was denoted as the S-0.1-PFKZ/GCE. The modified electrodes were dried under the infrared lamp before use. For comparison, the Pt/C/GCE was prepared according to the same method with suitable amount of catalyst (25 μg Pt/cm^2).

For RRDE experiments, the O_2 reduction voltammogram was obtained by performing a negative-direction sweep of potential from 1.164 V (*vs.* RHE) in 0.10 M KOH or from 1.056 V in 0.10 M $HClO_4$ at a rate of 5 mV/s, and the ring potential was set at 1.264 V in 0.10 M KOH or 1.056 V in 0.10 M $HClO_4$, respectively. Before experiments, all the electrodes were activated by potential cycling in 0.10 M $HClO_4$ from 1.056 to 0.144 V at a scan rate of 50 mV/s for 30 cycles.

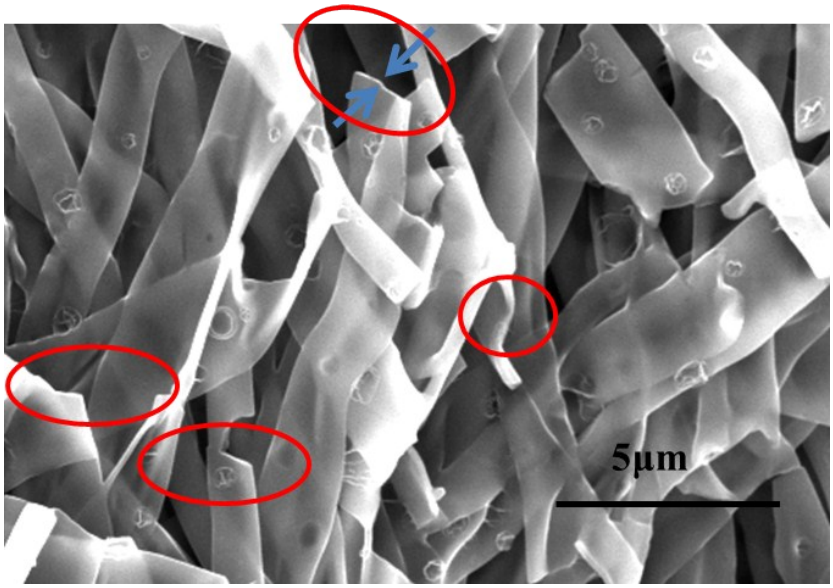

Figure S1. The SEM image of fracture surface of the S-0.1-PFKZ.

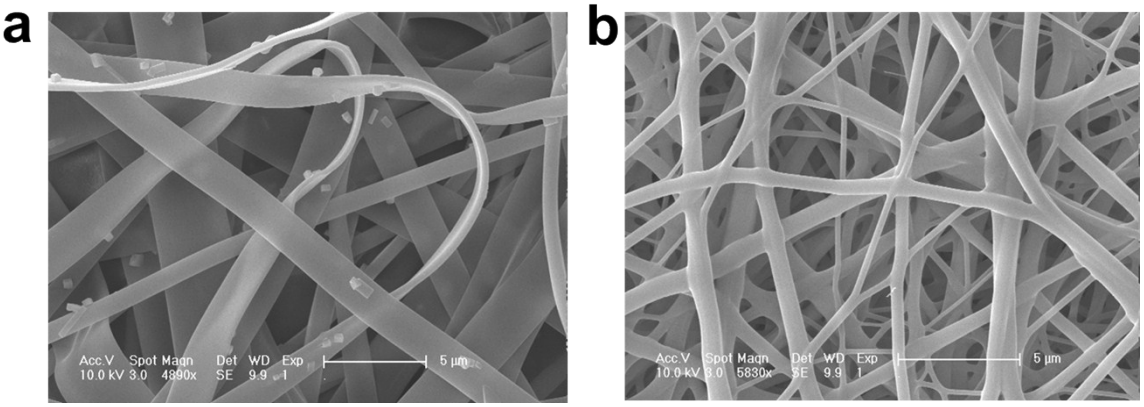

Figure S2. The SEM images of unheated (a) PFKZ and (b) PF materials.

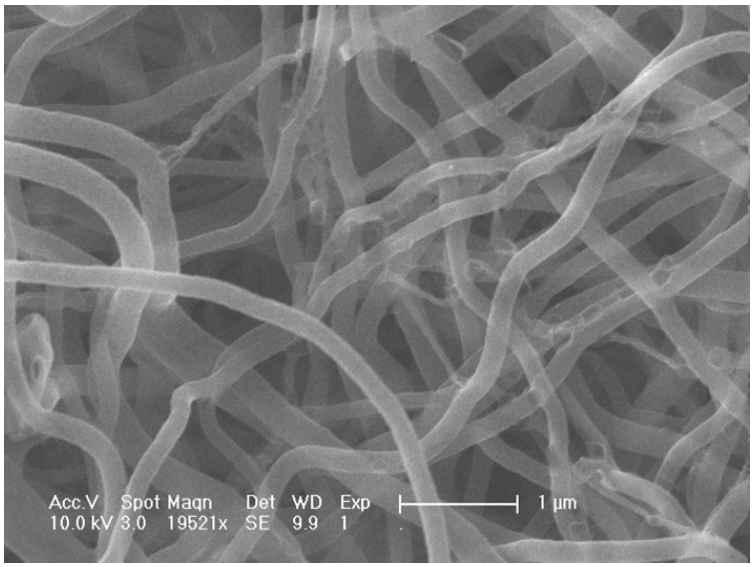

Figure S3. The SEM image of PFK.

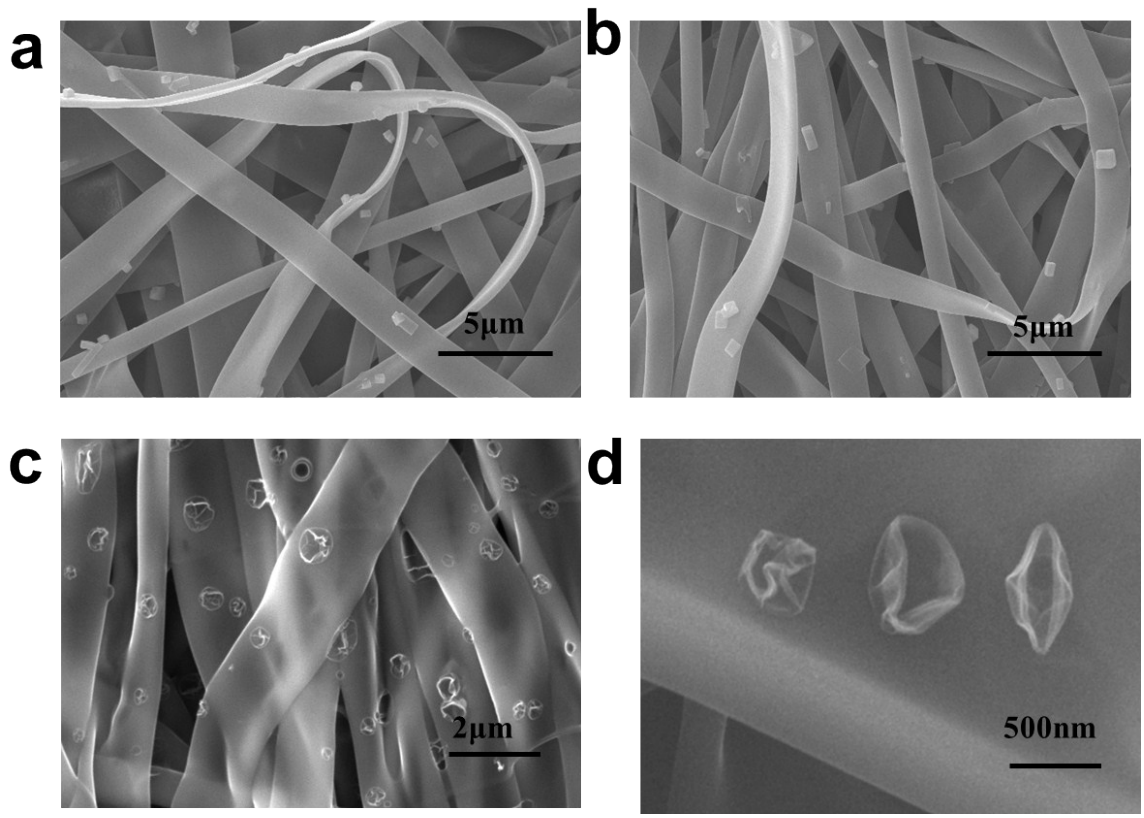

Figure S4. The SEM images of (a) unheated S-0.1-PFKZ, (b) muffle-treated S-0.1-PFKZ, (c) and (d) the resulting S-0.1-PFKZ in different magnifications.

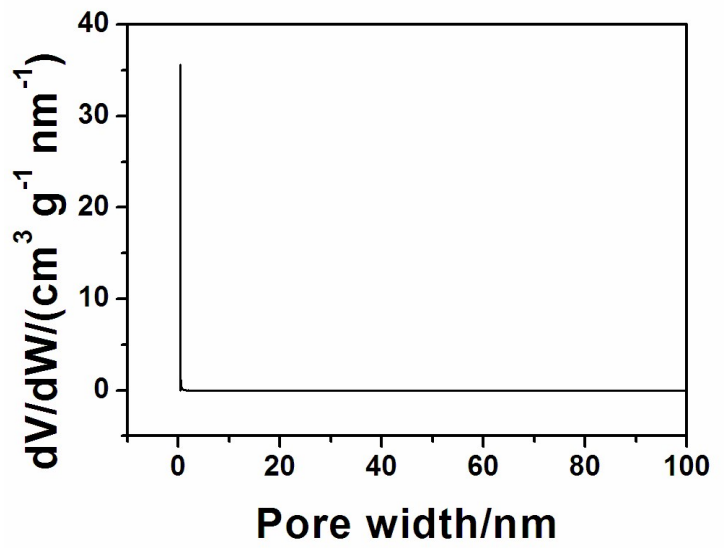

Figure S5. Pore size distribution of the S-0.1-PFKZ composite.

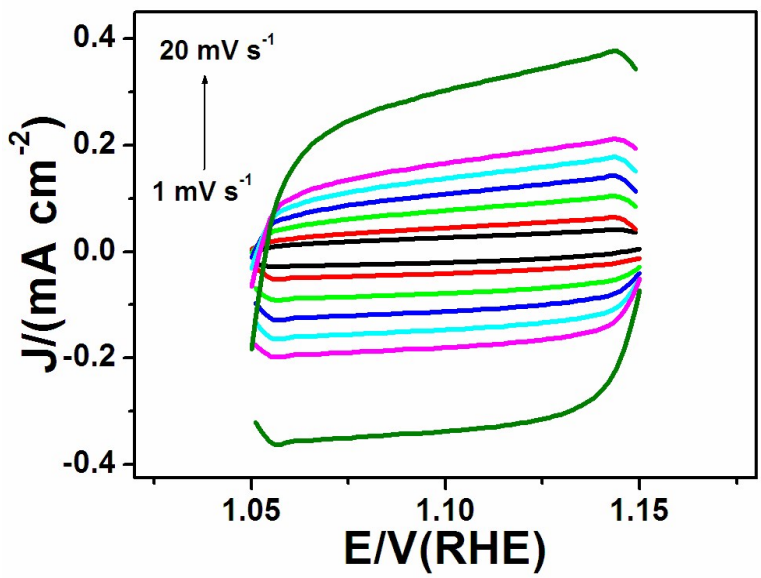

Figure S6. CVs of S-0.1PFKZ in 0.1 M KOH at different scan rates of 1, 2, 4, 6, 8, 10, 20 mV s^{-1}, respectively.

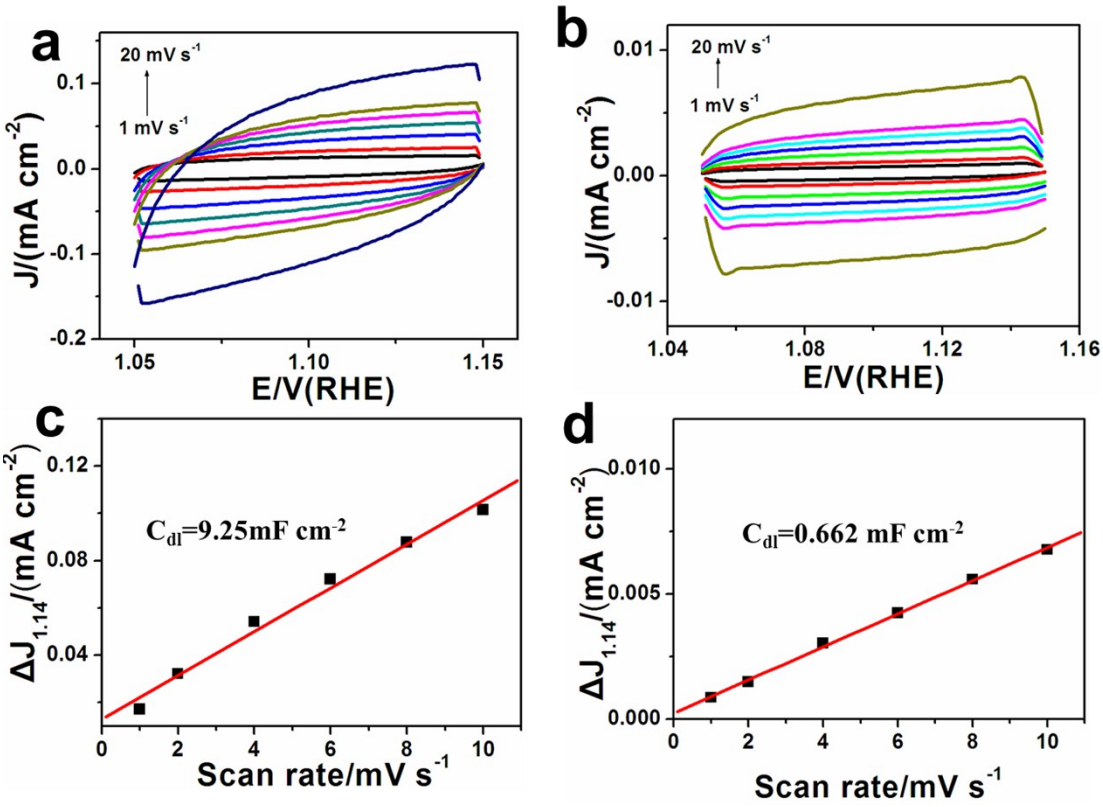

Figure S7. CVs of (a) PFKZ and (b) PF in 0.1 M KOH at different scan rates of 1, 2, 4, 6, 8, 10, 20 mV s^{-1}, respectively. (c) PFKZ and (d) PF, a plot of the ΔJ ($\Delta J = J_a - J_c$) at 1.14 *vs.* scan rates to determine the double layer capacitance (C_{dl}) and the roughness factor (R_f).

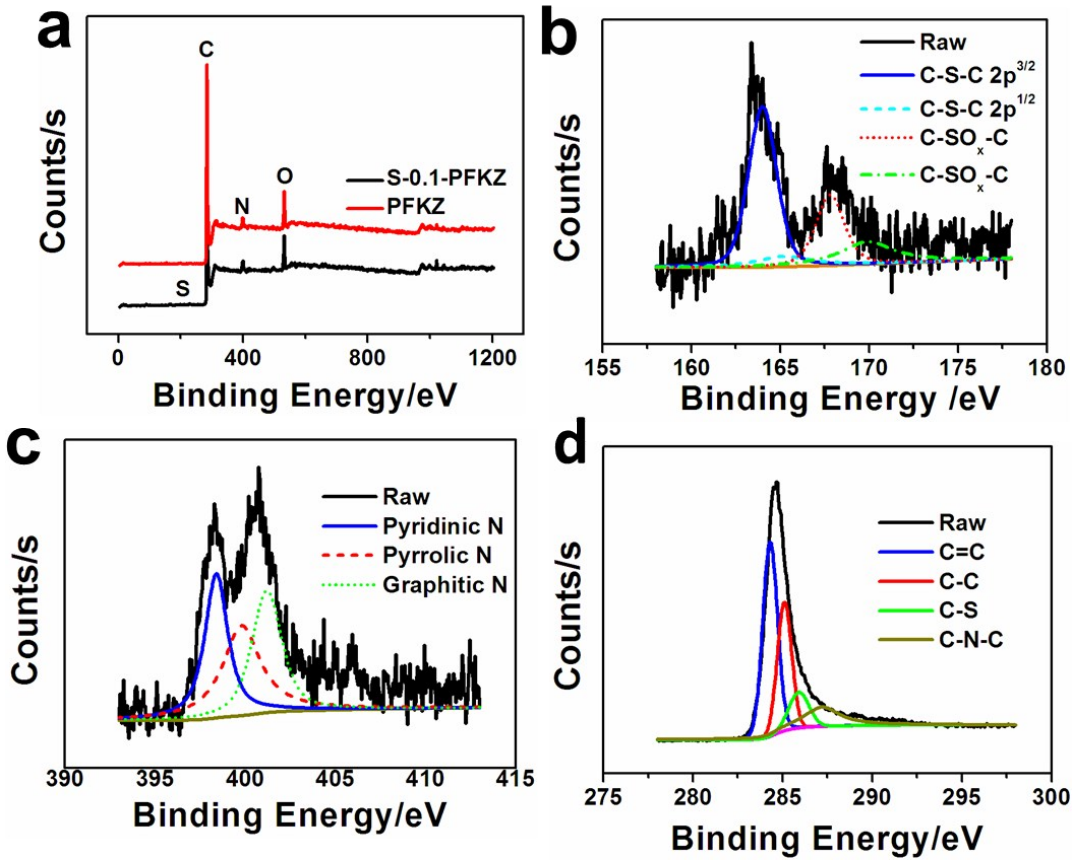

Figure S8. (a) XPS spectra of the resultant S-0.1-PFKZ and PFKZ, the high-resolution spectra of (b) S2p, (c) N1s, and (d) C1s in S-0.1-PFKZ.

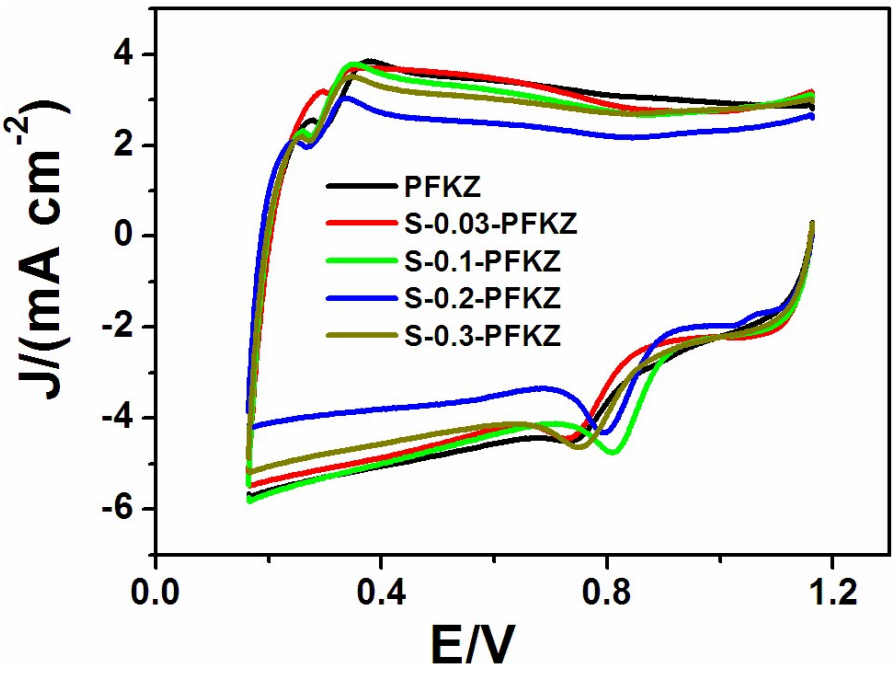

Figure S9. CVs of the PFKZ, S-0.03-PFKZ, S-0.1-PFKZ, S-0.2-PFKZ, and S-0.3-PFKZ in O_2-saturated 0.10 M KOH. Scan rate is 50 mV/s.

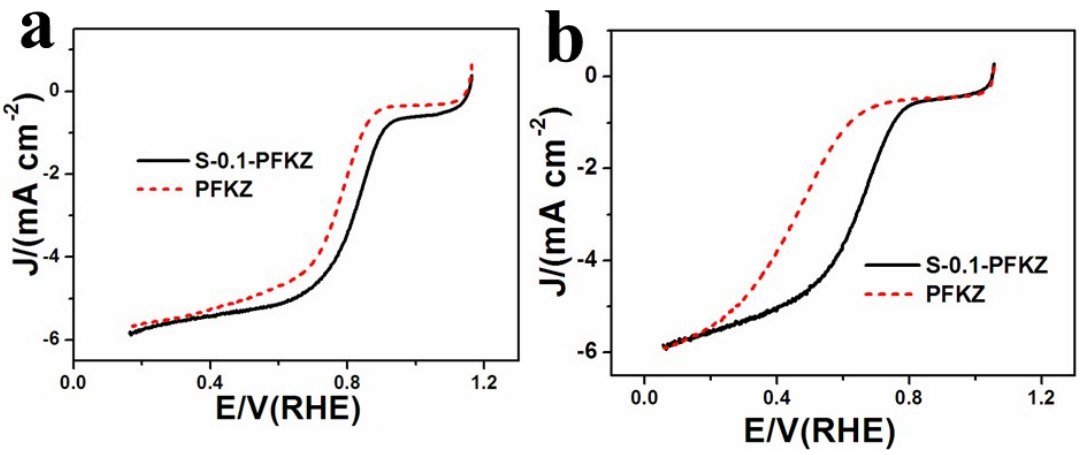

Fig. S10. (a) LSV curves of S-0.1-PFKZ and PFKZ in O_2-saturated (a) 0.10 M KOH and (b) 0.10 M $HClO_4$ at a scan rate of 5 mV/s, rotation rate = 1600 rpm.

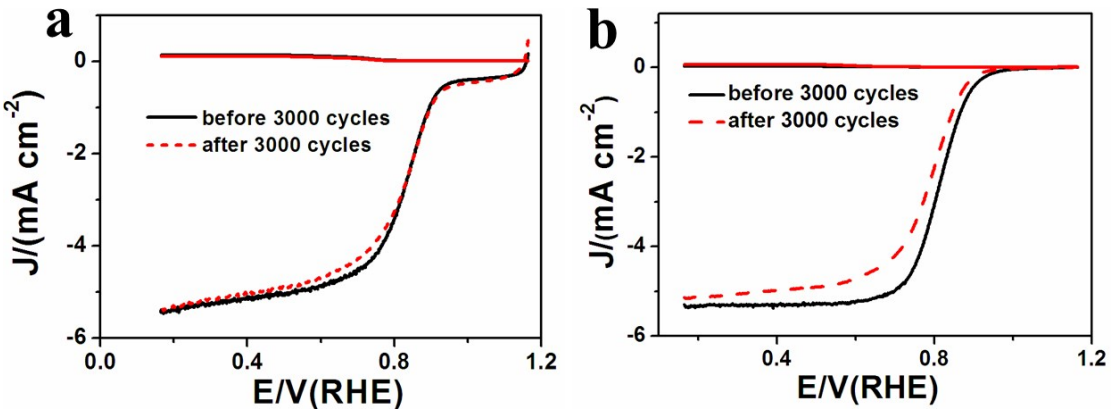

Fig. S11. LSV curves of (a) S-0.1-PFKZ and (b) Pt/C for ORR in O_2-saturated 0.10 M KOH before and after 3000 cycles.

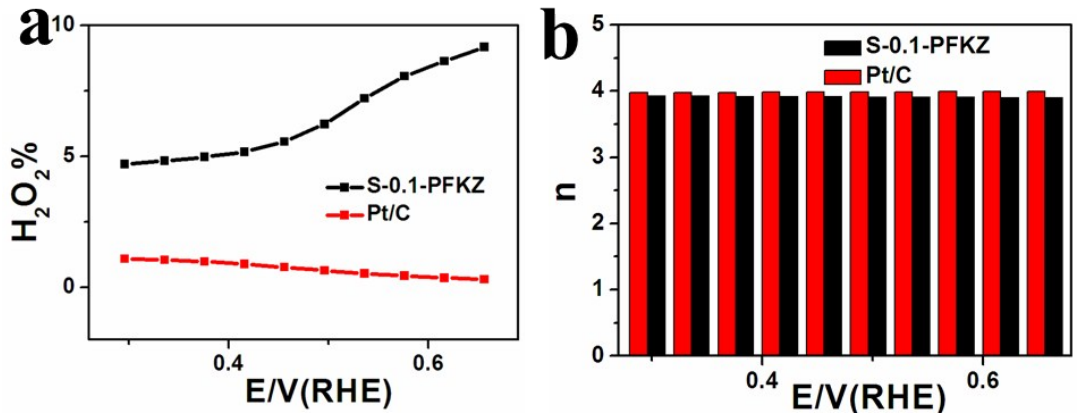

Figure S12. (a) H_2O_2 yield and (b) electron transfer number (n) of S-0.1-PFKZ and Pt/C in O_2-saturated 0.10 M $HClO_4$ at a scan rate of 5 mV/s, rotation rate = 1600 rpm.

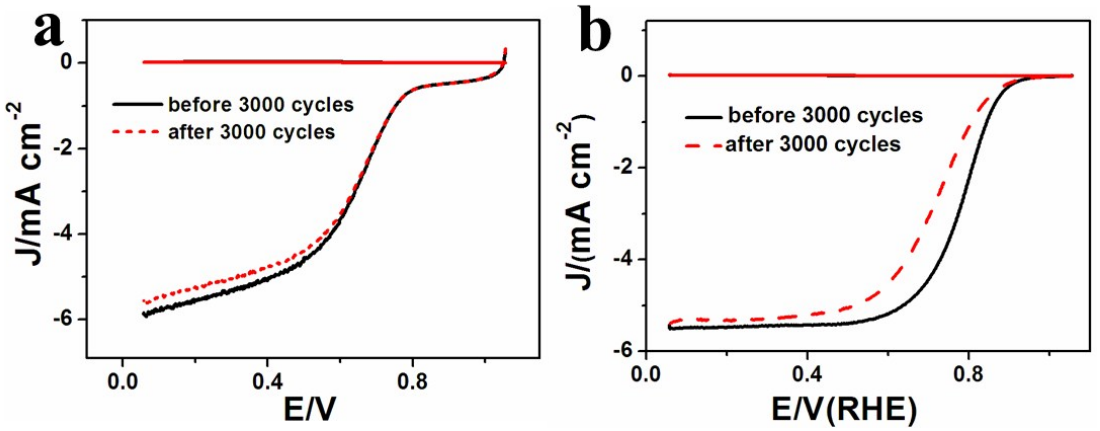

Fig. S13. LSV curves of (a) S-0.1-PFKZ and (b) Pt/C for ORR in O_2-saturated 0.10 M $HClO_4$ before and after 3000 cycles.

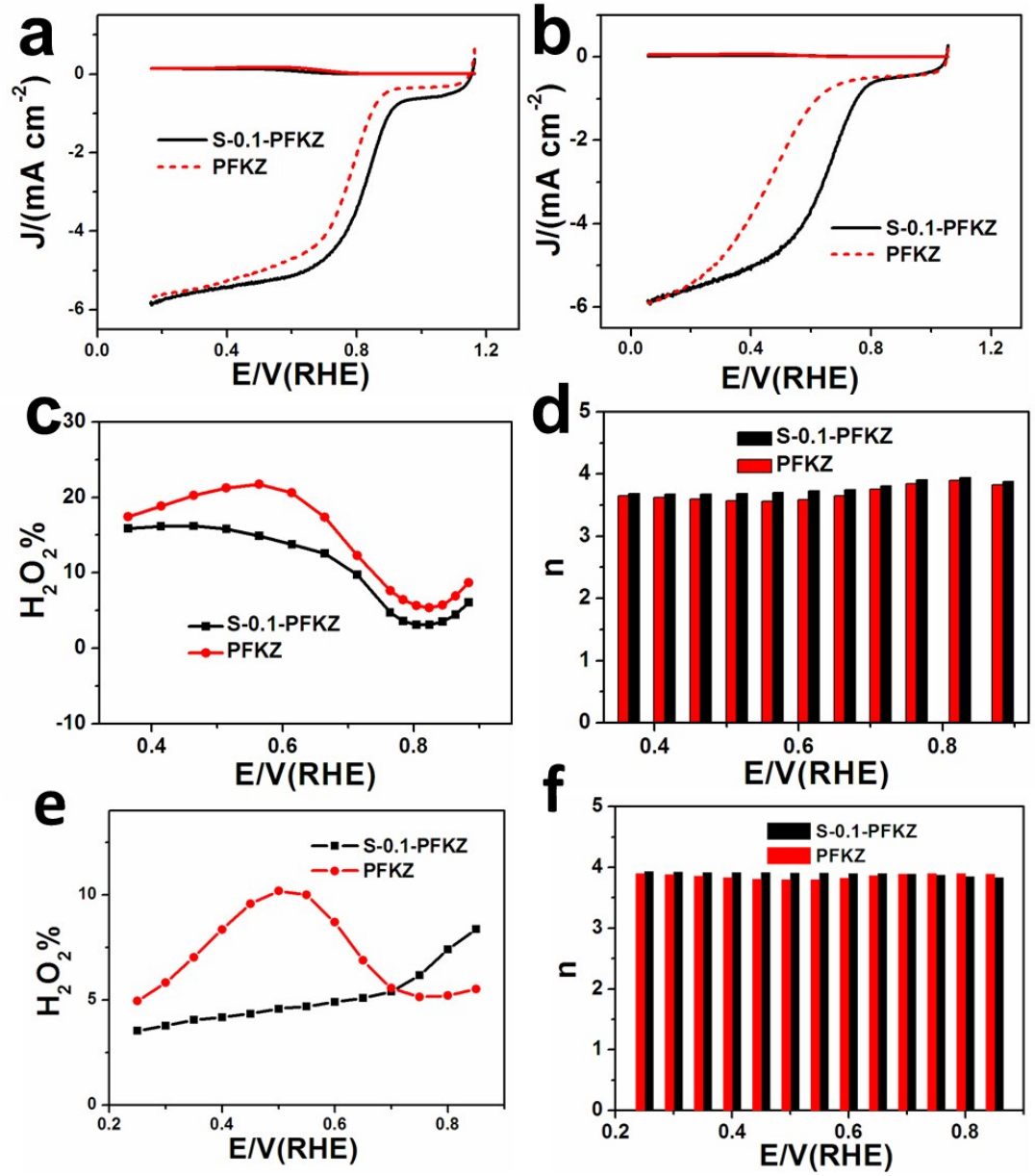

Figure S14. RRDE voltammograms of S-0.1-PFKZ and PFKZ in O_2-saturated (a) 0.10 M KOH and (b) 0.10 M $HClO_4$ at a scan rate of 5 mV/s, rotation rate = 1600 rpm. (c) H_2O_2 yield and (d) electron transfer number (n) of S-0.1-PFKZ and PFKZ in O_2-saturated 0.10 M KOH. (e) H_2O_2 yield and (f) electron transfer number (n) of S-0.1-PFKZ and PFKZ in O_2-saturated 0.10 M $HClO_4$.

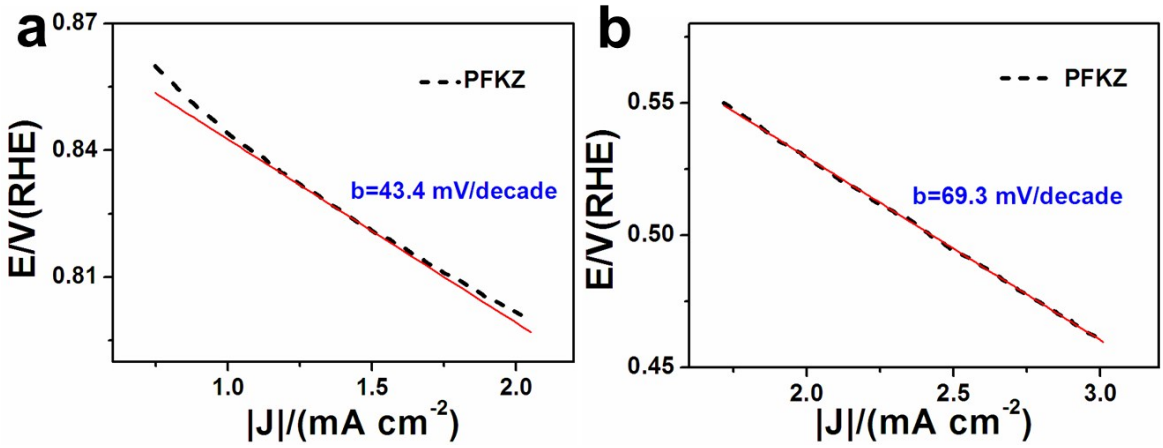

Figure S15. Tafel plots of PFKZ in O_2-saturated (a) 0.10 M KOH and (b) 0.10 M $HClO_4$.

Table S1. Comparison of BET surface area of our NSCNB with other reported nanofiber and nanobelt materials.

Electrospun materials	BET surface area/m^2 g^{-1}	References
N-$Fe_{0.5}C_{GO}$-800	37.4	1
TiO_2−G nanofibers	191 ± 5	2
GANF1	178.4	3
MSFs	0.24	4
Fe_3O_4/C	349.02	5
$LiFePO_4$/C	19.4	6
SnO_2 nanofibers	34.11	7
HfO_2 nanobelts	31.91	8
NSCNB	**535.3**	**This work**

GANF1: Ni catalyzed carbon nanofibers; **MSFs**: mesoporous silica fibers

Table S2. Comparison of ORR performance in basic and acidic media for NSCNB with other metal-free heteroatom-doped carbon electrocatalysts.

Catalyst	E^b_{onset}/V	$E^b_{1/2}$/V	E^a_{onset}/ V	$E^a_{1/2}$/V	Reference electrode	Ref.
S-graphene	-0.15	-0.37	-	-	vs. SCE	9
NOSCs	0.96	0.74	-	-	vs. RHE	10
S_2N_2-GN1000	-0.052	-	-	-	vs. Ag/AgCl	11
N,S-RGO/GQDs	-0.10	-	-	-	vs. Ag/AgCl	12
CNT/HDC-1000	0.92	0.82	-	-	vs. RHE	13
C-PANI/NSA	0.84	0.67	-	-	vs. RHE	14
N,S-graphene	-0.06	-	-	-	vs. Ag/AgCl	15
S,N-CNTs	Similar to Pt/C	-	0.56		vs. Ag/AgCl	16
SN/C-900	0.035	-			vs. Ag/AgCl	17
S-graphene-800	-0.15	-			vs. SCE	18
N,S-graphene	-0.05	-			vs. Ag/AgCl	19
NSCNB	**0.932**	**0.831**	**0.776**	**0.657**	**vs. RHE**	**This work**

E^b: potential in basic solution; **E^a**: potential in acidic solution;
NOSCs: N-, O-, and S-tridoped, polypyrrole-derived nanoporous carbons; **S_2N_2-GN**: N and S dual doped graphene; **RGO**: reduced graphene oxide; **GQDs**: graphene quantum dots; **HDC**: heteroatom-doped carbon; **PANI**: polyaniline; **NSA**: b-naphthalene sulfonic acid.

References

1. W. Yang, Y. Zhang, C. Liu and J. Jia, *J. Power Sources*, 2015, **274**, 595-603.
2. X. Zhang, P. Suresh Kumar, V. Aravindan, H. H. Liu, J. Sundaramurthy, S. G. Mhaisalkar, H. M. Duong, S. Ramakrishna and S. Madhavi, *J. Phys. Chem. C*, 2012, **116**, 14780-14788.
3. I. Martin-Gullon, J. Vera, J. A. Conesa, J. L. González and C. Merino, *Carbon*, 2006, **44**, 1572-1580.
4. R. Ravichandran, S. Gandhi, D. Sundaramurthi, S. Sethuraman and U. M. Krishnan, *J. Biomat.Sci. -Polym. E.* , 2013, **24**, 1988-2005.
5. C. Han, Q. Ma, X. Dong, W. Yu, J. Wang and G. Liu, *J. Mat. Sci.-Mater. El.* , 2015, **26**, 2457-2465.
6. D. Shao, J. Wang, X. Dong, W. Yu, G. Liu, F. Zhang and L. Wang, *J. Mat. Sci.-Mater. El.*, 2013, **25**, 1040-1046.
7. W. Q. Li, S. Y. Ma, J. Luo, Y. Z. Mao, L. Cheng, D. J. Gengzang, X. L. Xu and S. H. Yan, *Mater. Lett.*, 2014, **132**, 338-341.
8. Y. Su, B. Lu, Y. Xie, Z. Ma, L. Liu, H. Zhao, J. Zhang, H. Duan, H. Zhang, J. Li, Y. Xiong and E. Xie, *Nanotechnology*, 2011, **22**, 285609.
9. Z. Ma, S. Dou, A. Shen, L. Tao, L. Dai and S. Wang, *Angew. Chem. Int. Edit.*, 2015, **54**, 1888-1892.
10. Y. Meng, D. Voiry, A. Goswami, X. Zou, X. Huang, M. Chhowalla, Z. Liu and T. Asefa, *J. Am. Chem. Soc.*, 2014, **136**, 13554-13557.
11. J.-M. You, M. S. Ahmed, H. S. Han, J. E. Choe, Z. Ustundag and S. Jeon, *J. Power Sources*, 2015, **275**, 73-79.
12. Z. Luo, D. Yang, G. Qi, J. Shang, H. Yang, Y. Wang, L. Yuwen, T. Yu, W. Huang and L. Wang, *J. Mater. Chem. A*, 2014, **2**, 20605-20611.
13. Y. J. Sa, C. Park, H. Y. Jeong, S.-H. Park, Z. Lee, K. T. Kim, G.-G. Park and S. H. Joo, *Angew. Chem. Int. Edit.* , 2014, **53**, 4102-4106.
14. R. Zheng, Z. Mo, S. Liao, H. Song, Z. Fu and P. Huang, *Carbon*, 2014, **69**, 132-141.
15. J. Liang, Y. Jiao, M. Jaroniec and S. Z. Qiao, *Angew. Chem. Int. Edit.*, 2012, **51**, 11496-11500.
16. Q. Shi, F. Peng, S. Liao, H. Wang, H. Yu, Z. Liu, B. Zhang and D. Su, *J. Mater. Chem. A*, 2013, **1**, 14853-14857.
17. Y. Li, H. Zhang, Y. Wang, P. Liu, H. Yang, X. Yao, D. Wang, Z. Tang and H. Zhao, *Energ. Environ. Sci.*, 2014, **7**, 3720-3726.
18. J. Wang, R. Ma, Z. Zhou, G. Liu and Q. Liu, *Sci. Rep.*, 2015, **5**, 9304.
19. J. Liang, X. Du, C. Gibson, X. W. Du and S. Z. Qiao, *Adv. Mater.*, 2013, **25**, 6226-6231.